PROGRESS IN COLOR, COLORANTS AND COATINGS

available online @ www.pccc.icrc.ac.ir

Progress in Color Colorants Coating 18 (2025), 53-71

Ministry of Science, Research and Technology
Institute for Color Science & Technology

The Potential of Gundelia Seeds Waste as an Emerging Sustainable Adsorbent for Methylene Blue-Polluted Water Treatment

N. Albayati[1], M. Mohammed[1], H. Ahmed[2], M. Kadhom[*2]

[1.] Department of Chemical Engineering, College of Engineering, University of Baghdad, P.O. Box: 10071, Baghdad, Iraq.

[2.] Department of Environmental Science, College of Energy and Environmental Science, Alkarkh University of Science, P.O. Box: 10081, Baghdad, Iraq

ARTICLE INFO

Article history:
Received: 09 Mar 2024
Final Revised: 05 June 2024
Accepted: 08 June 2024
Available online: 20 July

Keywords:
Gundelia
Biomass adsorbents
Dye removal
Methylene blue
Wastewater treatment
Sustainability

ABSTRACT

Gundelia, a genus of flowering plants native to the Mediterranean region, particularly in Iraq, holds promise as a sustainable adsorbent for the treatment of dye-polluted water. This study explores the potential of Gundelia seeds (GS) waste as a biobased adsorbent for removing methylene blue dye from synthesized wastewater. Utilizing various analytical techniques, including scanning electron microscopy (SEM), Fourier transform infrared (FTIR) spectroscopy, and X-ray diffraction analysis (XRD), we assessed GS as an active adsorbent with performance comparable to fabricated and expensive composites. Key parameters such as pH (3-11), pH at the point of zero charge, temperature (298-328 K), dose (0.02-0.1 g), dye concentration (10-50 ppm), and contact time (10-40 min) were systematically investigated. The point of zero charge was determined to be at pH 8, with the highest removal efficiency observed at pH 11. A contact time of 30 minutes yielded a removal rate of approximately 90 %, with an adsorption capacity of 11.07 mg/g. The highest adsorption capacity, 30.57 mg/g, was attained under conditions of 50 ppm dye concentration, 0.02 g dose, and a 40-minute contact time. The study examined three isotherm models, namely Langmuir, Freundlich, and Temkin; all demonstrating a high fit, with Langmuir exhibiting preferability. On the other hand, five kinetic models were explored; the Pseudo second-order model provided the most accurate description of the adsorption process. Prog. Color Colorants Coat. 18 (2025), 53-71© Institute for Color Science and Technology.

1. Introduction

Approximately 2.2 billion individuals globally lack access to potable water, with an additional 800 million facing inadequate drinking water provisions due to water scarcity and excessive utilization [1]. The prevalence of water scarcity is noticeably escalating in Southeast Asia, primarily attributed to climate change [2]. The expected effects on water supplies in the Middle East and North Africa (MENA) region include population growth, economic expansion, climate fluctuations, and environmental consequences. Employing advanced hydrological and water allocation models in a bifurcated simulation process reveals a forecasted total water demand of 393 km^3 annually by 2050, accompanied by an associated water deficit of 199 km^3 yearly under standard climate change scenarios. The surge in demand by 50 %, coupled with a 12 % reduction in supply, contributes to this discernible escalation. Nine General Circulation Models (GCMs) indicate an anticipated water shortfall for 2050 in the range of 85-283 km^3/yr.

*Corresponding author: * kadhom@kus.edu.iq
mohammedkadhom@gmail.com
https://doi.org/ 10.30509/pccc.2024.167290.1285

The study attributes 78 % of water scarcity to evolving socioeconomic conditions, while climate change is accountable for the remaining 22 % [3].

Dyes are broadly categorized into cationic, anionic, and nonionic types. Cationic dyes involve basic dyes, while the anionics include acid, reactive, and direct. The nonionic dyes comprise diffused dyes [4]. Methylene blue (MB) stands out as an intricately structured, positively charged stain, posing challenges in removal processes [5]. It has versatile applications across various industries, including garment manufacturing, as well as the chemical, pharmaceutical, and biological sectors. Methyl orange (MO) shares a chemical structure with MB, exhibiting similar molecular mass, and is extensively employed across various industries [6]. Methyl red, akin to methyl orange, is an azo dye characterized by substantial molecular weight, presenting difficulties in elimination. Removing other acidic and basic dyes is also imperative in the treatment process [7].

Various techniques are employed for the remediation of water contaminated with dyes, including filtration, coagulation, electrochemical removal, photocatalysis, ultrasonic and biological breakdown, chemical oxidation, and adsorption [8, 9]. Among those, adsorption is a process wherein certain chemicals or ions adhere to the surfaces of a solid substance (adsorbent) and offers several advantages. It is featured for its ease of use, high efficiency, and the absence of hazardous byproducts. Diverse materials have been utilized as adsorbents for different compounds in previous studies [10, 11]. Notably, the cost-effectiveness of adsorption, ranging from $5 to $200 per cubic meter of treated water, is one of the most effective factors when compared to alternative water purification methods, which cost around $10 to $450 per cubic meter [12, 13]. Furthermore, it is user-friendly, efficient, renewable, and environmentally benign. After a thorough evaluation of the benefits and drawbacks associated with various approaches, research teams often designate adsorption as the optimal choice [14].

Biomass waste, particularly agricultural residue, has recently garnered significant attention as a promising agent for stain removal. The proliferation of the food industry, directly correlated with the expanding global population, is a substantial contributor to this waste stream. The appeal of biowaste lies in its economic viability, extensive availability (generated wherever human habitation occurs), and demonstrated effectiveness, rendering it a valuable resource for adsorbent fabrication. The utilization of this resource in the adsorption process encompasses on-site consumption, adsorbent production, operation, and/or regeneration [15]. Various agricultural byproducts, including peels, leaves, seeds, and more, can be transformed into nanomaterials through thermal treatment [16]. Some of these materials have been employed directly, without undergoing additional processing, while others have been utilized in modified forms.

Many researchers, including us, have delved into the investigation of biowaste. However, a limited focus has been on exploring natural plants as bio-based adsorbents for wastewater treatment. The natural cycle of drying and decomposition following the growing season offers an opportunity to utilize the remnants of these plants as effective adsorbents. Found in diverse habitats, these plants often follow a seasonal cycle. While there exists a broad spectrum of research on plants from various botanical families, some have undergone extensive examination, while others have been relatively overlooked. Depending on their efficacy, these commonly growing plants have the potential to serve as cost-free repositories for a variety of adsorbents.

Gundelia is known for its traditional medical applications; recently, Dalar et al. [17] studied the Gundelia rosea seeds' biopharmaceutical potential and bioactive compounds. The outcomes affirm the common use of Gundelia rosea and indicate its ability as a novel candidate for biopharmaceutical agents addressing general health concerns. The cypselas of Gundelia are rich in fatty acids, comprising approximately 7% oleic acid and 12.5 % linoleic acid. This composition renders the oil derived from these cypselas comparable to oils from well-known sources such as soybean, corn, sunflower, and sesame [18]. The utilization of Gundelia seeds in removing heavy metals was reported, where Shandi et al. [19] explored the potential of using Gundelia tournefortii as a low-cost biosorbent to terminate Cu (II) ions from synthetic aqueous solutions. Batch-mode tests examined pH, biosorbent dosage, temperature, contact time, and initial Cu (II) concentration. The Langmuir equation best-described biosorption, with 38.76 mg/g adsorption capacity; the kinetic study showed that the pseudo-second-order model described adsorption kinetics. Thermodynamic measurements indicated spontaneous and exothermic biosorption. Similarly, Rahimpour et al. [20] removed

Pb(II) from wastewater using Gundelia tournefortii. The Langmuir isotherm accurately described biosorption, demonstrating a single-layer maximum adsorption capacity of 144.93 mg/g at 20 °C. Also, the pseudo-second-order was suitable to describe the kinetics. The sorption process was spontaneous, practicable, random, exothermic, and physical, according to thermodynamic analysis. However, Mokhtaryan et al. initiated a Gundelia tournefortii seed-activated carbon that efficiently removed acetaminophen from synthetic solutions. The optimal conditions for maximum removal (98.3 %) were 30 minutes, 20 mg/L Ca (II), pH 4.0, 0.25 g/L adsorbent, and 25 °C [21]. In the same context, Pezeshkvar et al. [22] fabricated a new nanocomposite based on NiO‑MWCNT‑sodiumdodecyl sulfate synergized with Gundelia tournefortii extract and used it as a catalyst.

In this study, the waste of Gundelia Seeds, also called tumble thistle and locally known as Sissi, was utilized as an adsorbent for the removal of MB from simulated wastewater using a batch method. Diverse operational configurations and characterization techniques were employed to identify the optimal conditions and assess the performance of the plant. Remarkably, the plant exhibited outstanding performance compared to its baseline application, achieving a removal efficiency of over 90% across all investigated parameters. This success has motivated our research group to undertake a comprehensive exploration of this plant in our upcoming project.

2. Experimental

2.1. Chemicals

Gundelia seeds were sourced from the local market in Baghdad, with the aim of collecting their waste for adsorption applications after eating the seeds. The MB dye possessed a molecular weight of 319.86 g/mol and a chemical formula of $C_{16}H_{18}ClN_3S\ xH_2O$; it was procured from R&M Chemicals, India. Distilled water was employed to prepare dye-aqueous solutions throughout the experimental procedures. Sodium hydroxide (NaOH) and hydrochloric acid (HCl, 37 %) were also bought from R&M Chemicals. The dye solution underwent centrifugation using a PLC-03-GEMMY centrifuge system from Taiwan to achieve effective separation between the adsorbate and adsorbent. Detection of the dye was performed employing a UV-Vis-T80-PG Ultraviolet-Visible (UV-Vis) spectrophotometer manufactured by Oasis Scientific Inc., UK.

2.2. Adsorbate solution

The initial solution was fit by dissolving MB dye powder in a concentration of 1 g in 1 L of deionized (DI) water within a volumetric flask, yielding a stock solution of 1000 ppm concentration. Subsequent concentrations of dye adsorbates were attained by diluting the original solution with DI water. To achieve the aimed pH levels, alkaline and acidic solutions were generated using diluted aqueous solutions of sodium NaOH and HCl with a concentration of 0.1 M. The pH adjustments were carried out utilizing a calibrated pH meter sourced from Mettler Toledo in Hamilton, New Zealand.

2.3. Adsorbent preparation

After collecting the plant's waste, it underwent through a DI water rinse to eliminate potential saliva (from eating), dust, and contaminants. Following this, an acidic pH water solution was employed to thoroughly clean the collected inflorescence, eliminating any potential biological impurities and germs. The plant then underwent immersion and multiple rinses with deionized water to restore its natural state. Subsequently, the plant was subjected to a temperature of 60 °C in an oven for 12 hours. The waste was pulverized using a mill to reduce the waste's size, and the resulting material was filtered through a 250 µm mesh. A secondary drying process was carried out in the oven at a temperature of 60 °C for 12 h. The final product was carefully stored in an airtight container to prevent moisture ingress. Figure 1 illustrates the various stages of the preparation process.

2.4. Characterization of prepared powder

A Bruker company FTIR spectrometer, model IFS 125HR, was utilized to capture spectra between 4000-400 cm^{-1}. The morphology of the particles was examined by scanning electron microscopy (SEM) with an accelerating voltage of 15 kV. This examination technique was conducted using an Inspect S50 microscope from the FEI Company in the Czech Republic. Our samples were also characterized using the X-ray diffraction (XRD) technique via Panalytical X pert, 2012 (The Analytical X-ray Company, Netherlands).

Figure 1: Stages of the preparation process for the plant's waste powder.

2.5. Batch set up

The batch equilibrium study incorporated various factors, namely initial dye concentration (applied from 10 to 50 mg/L), solution pH (adjusted between 3 and 11), GS dosage (ranging from 0.02 to 0.1 g), and temperature (set between 25 and 55 °C). A Karl Kolb shaker from Germany consistently oscillated all samples at 350 rpm. pH adjustments were made applying either 0.1 M NaOH or HCl. The point of zero charge was also studied, where conditions of 30 min time, DI water, 0.06 g dose, and 350 rpm mixing rate were applied. Data were collected at different intervals until reaching equilibrium, and a UV-Visible spectrophotometer was employed to calculate the MB concentration. MB's wavelength was set at 668 nm at all conditions [23]. For normal operation, the temperature and pH were room temperature (RT) and 7, respectively.

The removal rate and adsorption capacity (q_e) of MB were estimated using the formulas outlined by Kalash et al. (Eqs. 1 and 2) [24].

$$R\% = \frac{C_o - C_f}{C_o} \times 100\% \quad (1)$$

$$q_e = \frac{V\,(C_o - C_f)}{m} \quad (2)$$

Here:
C_0: Initial MB concentration (mg/L).
C_f: Final MB concentration (mg/L).
V: Volume of the MB solution (liters).
m: Mass of the GS (grams).

2.6. Studying the kinetics

Examining the kinetics of adsorption provides insights into the chemical pathways and the interactions between powder and dye. The kinetic behavior was conducted by changing the contact time from 10 to 40 min. At the same time, other conditions of neutral pH, 350 rpm, RT, 30 ppm dye concentration, and 0.06 g GS/ 25 mL solution were applied. The kinetics were investigated using five models, namely: pseudo-zero-order, pseudo-first-order, pseudo-second-order, Elovich, and intraparticle diffusion. The equations and parameter definitions of the used models are clarified in our previous publication [24].

2.7. Studying the isotherm

At optimal conditions and various dye concentrations, Langmuir, Freundlich, and Temkin isotherms were employed to analyze the equilibrium adsorption of the MB. The applied conditions in this test were 0.06 g/ 25 mL dose, 30 min contact time, 350 rpm mixing speed, RT, natural pH, and varied MB concentration in the range of 10-50 ppm. Again, the details of those used models were listed in our previous work [24].

3. Results and Discussions

3.1. GS characterization

3.1.1. SEM test

SEM test for the morphology was conducted to examine the morphology of GS powder before and after adsorption of the MB. Here, images of two scales, 200 and 50 µm, were captured for the plain, 30 ppm dye-solution exposed, and 50 ppm dye-solution exposed GS. Before capturing the images, the samples exposed to the dye were collected, dried at 60 °C, and stored until examination. The images show that the GS powder is shaped like silks, which comes from its original skin nature. From the images of plain GS (Figures 2 a and b), it can be noted that the diameter of 10-15 µm. However, after adsorption, a slight increase in the diameter is observed, where the diameter ranges from 10-20 µm. This might be attributed to the dye uptake within the structure. Also, when the GS was exposed to high dye concentration, an accumulation occurred.

3.1.2. FTIR

The adsorbent surface underwent FTIR analysis to ascertain the specific functional groups. FTIR spectra, depicted in Figure 3, were examined within a wavelength range of 400 to 4000 cm^{-1}, unveiling numerous peaks associated with the adsorbent material. Here, these samples were examined, namely: the plain, exposed to 30 ppm dye-solution, and exposed to 50 ppm dye-solution. By comparing the three spectra, three notable peaks appear in the dye-adsorbed samples at 1100, 1365, and 1600 cm^{-1}, which get higher intensity as the concentration increases. The presence of these peaks can be attributed to the formation of modes resulting from hydrogen bonds of the N_{het}=HO type, stretching vibrations of the $C=S^{+}$ heterocycle, and vibrations of the unsaturated $C_{het}=N^{+}(CH_3)_2$ bond [25].

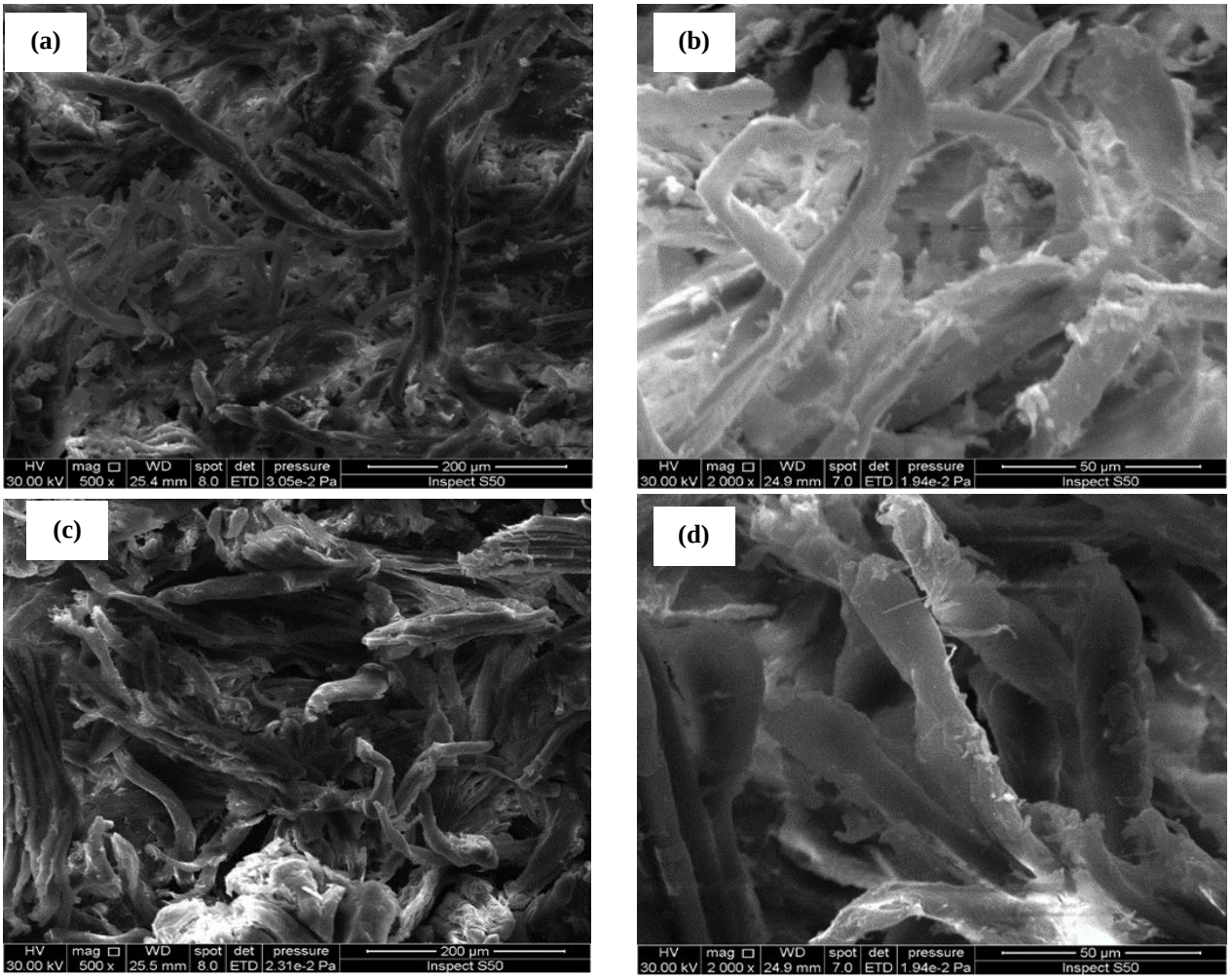

Figure 2: SEM images for different scales for the plain GS (a) and (b), after exposing to 30 ppm dye solution (c) and (d), and after exposing to 50 ppm dye solution (e) and (f).

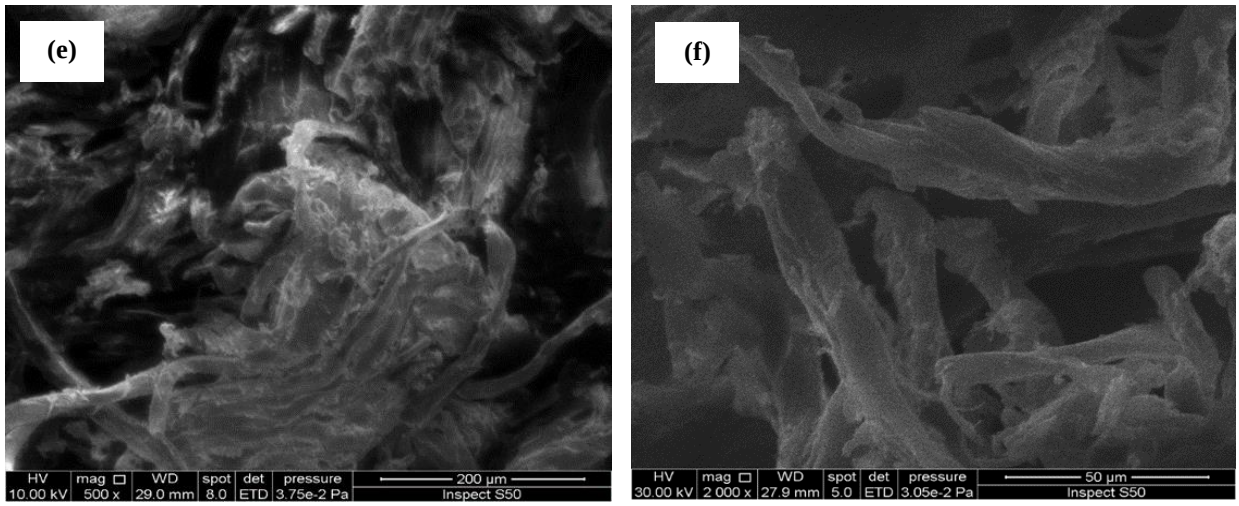

Figure 2: Continue.

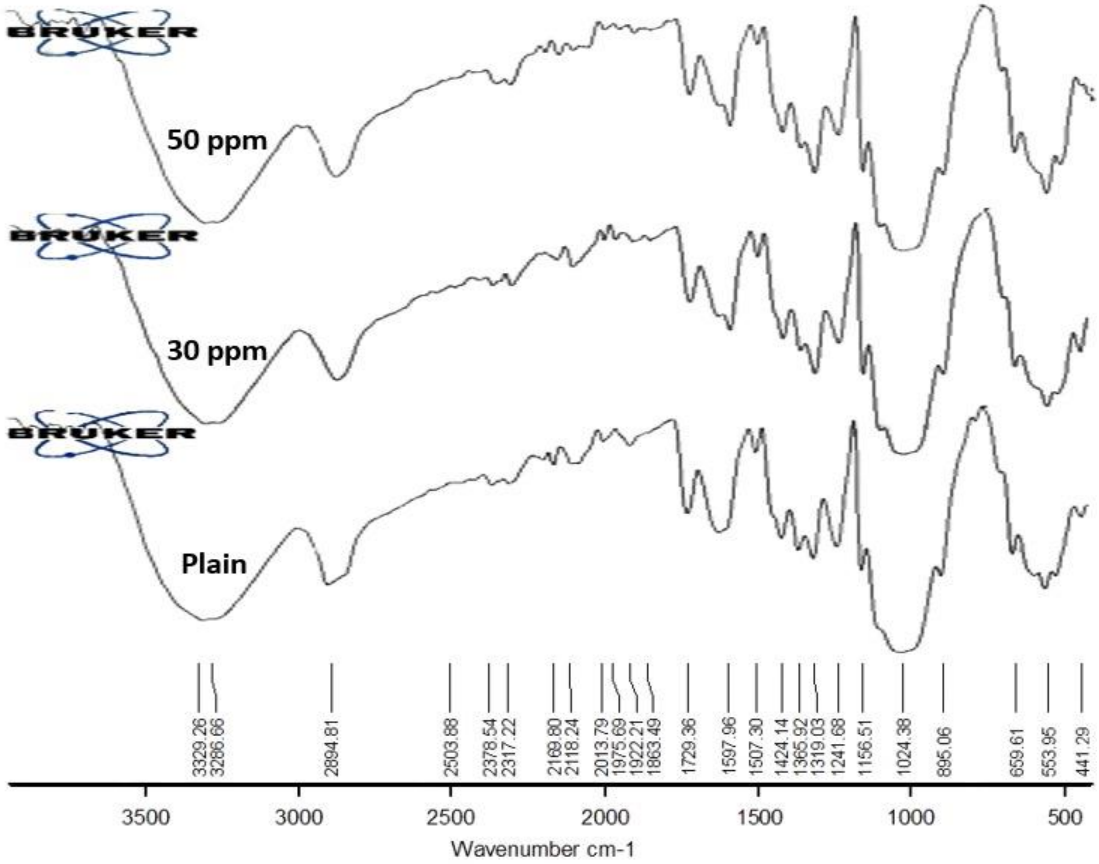

Figure 3: FTIR spectra of the plain, 30 ppm dye-solution adsorbent, and 50 ppm dye-solution adsorbent GS.

3.1.3. XRD

XRD emerges as a highly efficient technique for material characterization, particularly in the assessment of phase composition and crystal structure. In Figure 4, the XRD pattern is presented for the plain, 30 ppm dye-solution adsorbent, and 50 ppm dye-solution adsorbent GS. To achieve this, the adsorbent sample underwent Cu-Kα X-ray radiation (wavelength: 1.54 Å) at 40 kV and 44 mA. The acquisition of XRD data was carried out over a 2θ diffraction range from 20° to 80°. The appearance of peaks at 2θ = 22.5° and 73° in the XRD spectra mostly signaled the presence of the amorphous structure, although the peak at 73° was sharp. Variations in diffraction peak intensity are attributed to

the amorphous structure and differing degrees of hydration within the adsorbent. According to the figure, the structure was not affected after adsorption.

3.2. Adsorption operation factors

In the experimental section, the impact of physical factors, including pH, the pH of point zero charge (PZC), dye concentration, adsorbent dose, and solution temperature, on the rate of removal and adsorption capacity were investigated. The selection of operation conditions was primarily investigated as illustrated in the supplementary information, where the relationships of time and dye concentration were investigated by changing the adsorbent dose. The removal rate and adsorption capacity relationships after adding 0.02 g of the GS are illustrated in Figures S1 (a) and (b), respectively. Similarly, after filling 0.04, 0.06, 0.08, and 0.1 g, these relationships are graphed in Figures S2, S3, S4, and S5, respectively. However, the detailed findings of each factor are listed below.

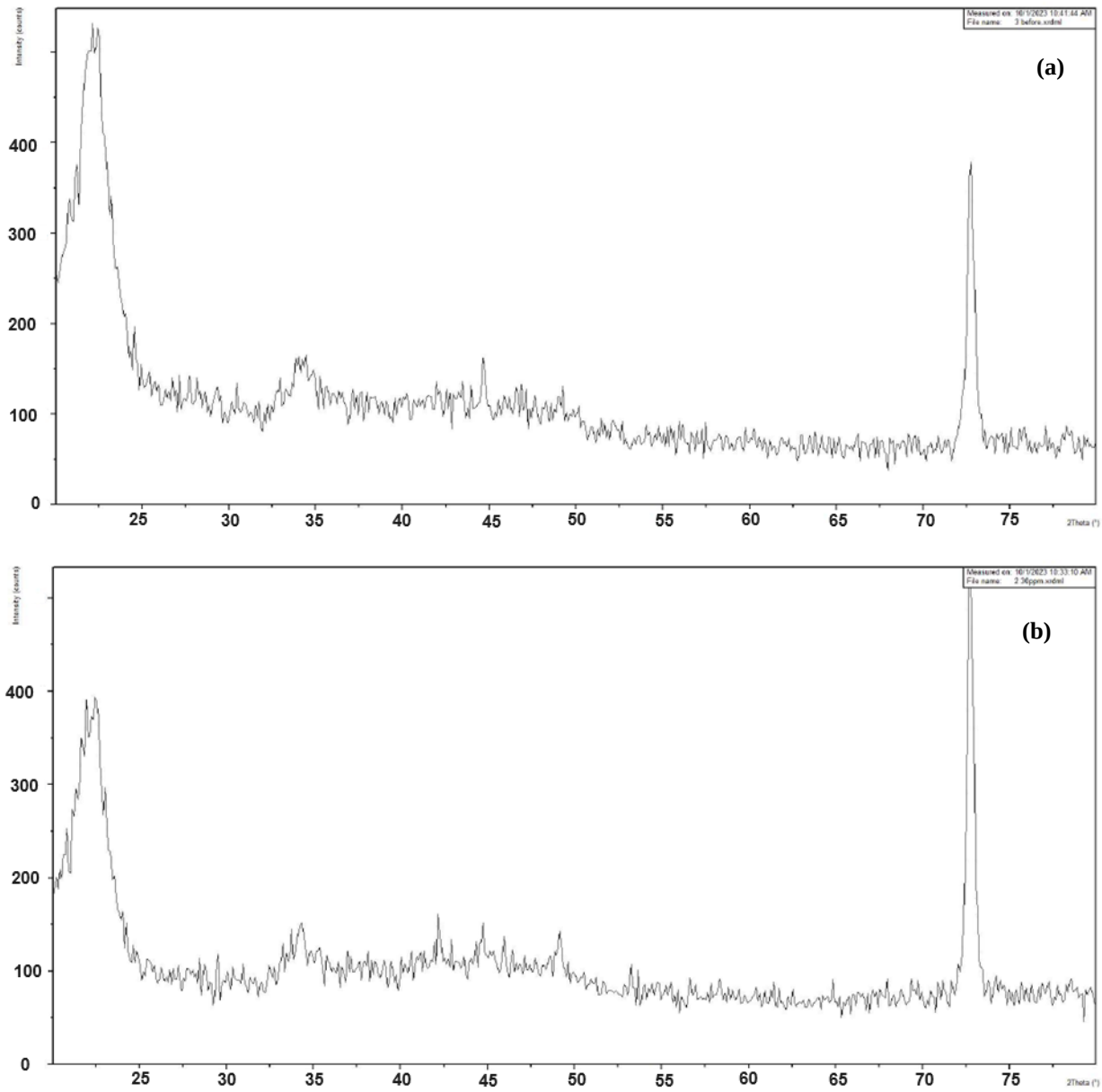

Figure 4: XRD test for (a) plain GS, (B) dye-adsorbed GS of 30 ppm, and (c) dye-adsorbed GS of 50 ppm.

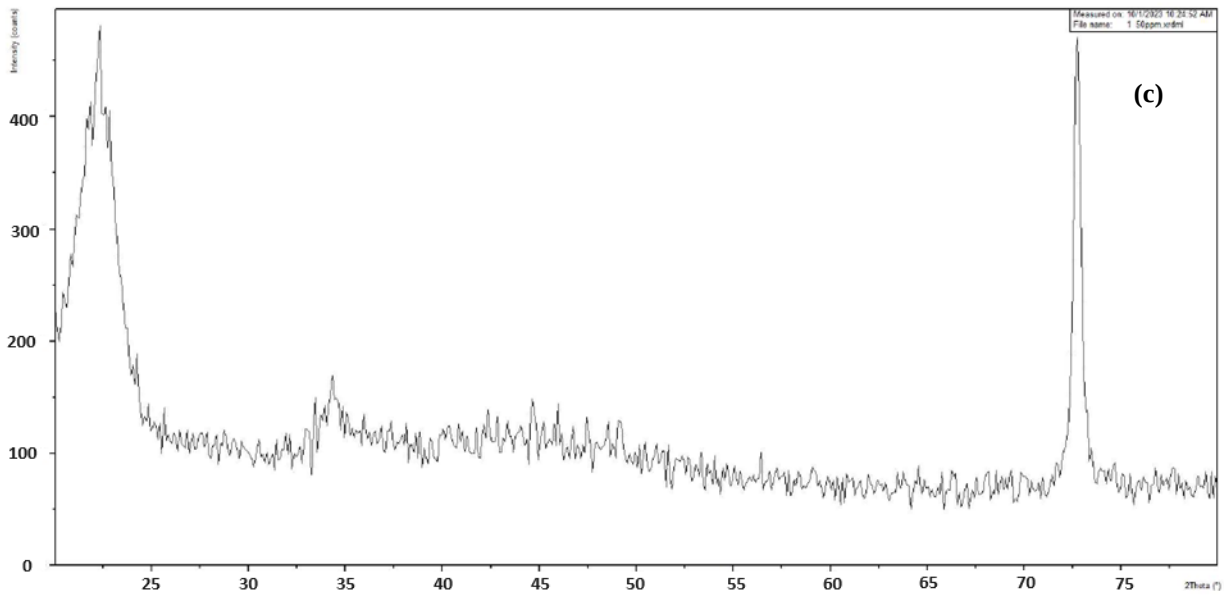

Figure 4: Continue.

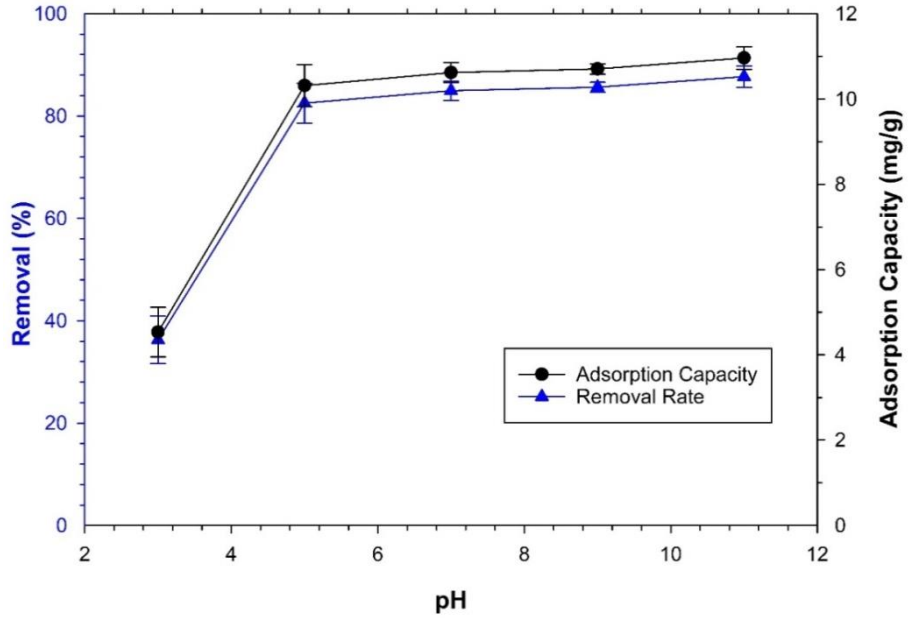

Figure 5: Effect of pH on the removal rate and adsorption capacity.

3.2.1. pH effect

An investigation was conducted to elucidate the influence of pH on the termination of dye as it is a pivotal determinant affecting both adsorbate and adsorbent. The studied pH, ranging from 3 to 11, was meticulously examined for its consequential effects. Variations in pH can exert influence on dye adsorption by modulating the surface charge of the adsorbent and the dissociation of dyes in the solution. Consequently, this investigation of pH aimed to discern its impact on the adsorbed dye, excluding the involvement of an adsorbent. Diverse solutions were prepared with varying pH levels. The solutions, containing a dye concentration of 30 mg/L, were agitated at 350 rpm and room temperature for 30 min, employing 0.06 g adsorbent/ 25 ml solution. The variation in pH values unveiled discernible changes in dye removal rates and adsorption capacities. This phenomenon might be attributed to the discernible influence of pH on the chemical structure of the dye, thereby affecting its color intensity [26].

Figure 5 delineates the impact of solution pH on the

removal rate and adsorption capacity at pH values of 3, 5, 7, 9, and 11. Notably, at a pH of 3, the minimum removal occurred, indicating the adverse effects of an acidic milieu. This trend aligns with the prevailing positive charge on the adsorbent surface at low pH levels, leading to electrostatic repulsion between the cationic dye and positively charged ions in the solution [27].

The optimum removal rate and adsorption capacity were observed at a pH of 7, succeeded by stability at larger pH values. This stability is attributable to the potential loss of hydrogen ions by MB molecules, inducing deprotonation. Consequently, the dye molecule acquires a negative charge, diminishing its affinity for negatively charged surfaces. Anionic dye molecules, in turn, undergo surface repulsion, precluding both adsorption and possible absorption [28, 29]. Optimal dye removal conditions are achieved near neutral pH levels, countering repulsive forces and minimizing interactions between dye molecules and surfaces. Remarkably, the adsorption process displayed rapid kinetics; here, around 85% of equilibrium capacity was attained at pH = 7. Additionally, the adsorption capacity followed the same behavior, where it reached 10.62 mg/g.

3.2.2. pH at the point of zero charge

The point of zero charge (PZC) is the pH at which a material's surface has no net electrical charge. It is a crucial factor in studying colloidal systems, affecting processes like adsorption and ion exchange [30]. For acidic PZC, when pH is below the PZC, the surface is positively charged; when above, it becomes negatively charged. In contrast, alkaline PZC denotes the pH where the surface is negatively charged. In acidic conditions, the surface tends to become positively charged, impacting adsorption and ion exchange. In alkaline conditions, the surface may acquire a negative charge at higher pH values, influencing these processes [31]. Figure 6 shows the PZC by plotting the pH_f-pH_i with pH_i. From the figure, the PZC is observed at an initial pH of 8. This value is slightly alkaline, where below this pH, the material's surface charge tends to be positive, and vice versa.

3.2.3. Dose effect

To scrutinize the effect of the adsorbent on the adsorption process, varying quantities of GS (ranging from 0.02 to 0.1 g) were employed in a sample volume of 25 mL. The experiments were performed at room temperature at a mixing rate of 350 rpm, maintaining a dye concentration of 30 ppm. Figure 7 elucidates the discernible influence of removal rates and adsorption capacity at 30 min of contact time. The highest dosage yielded a removal rate of 92.32 %, whereas the lowest dosage achieved a removal rate of 72.2 %.

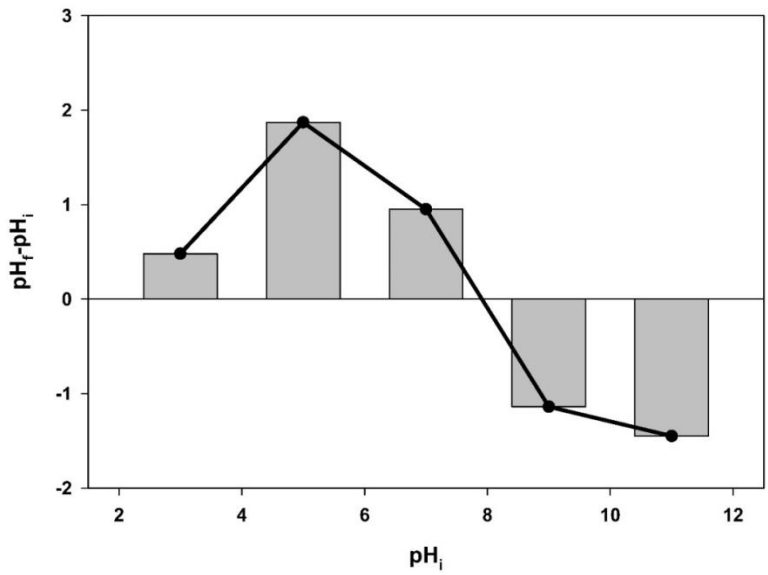

Figure 6: The relationship of pH_f-pH_i with pH_i for the determination of PZC.

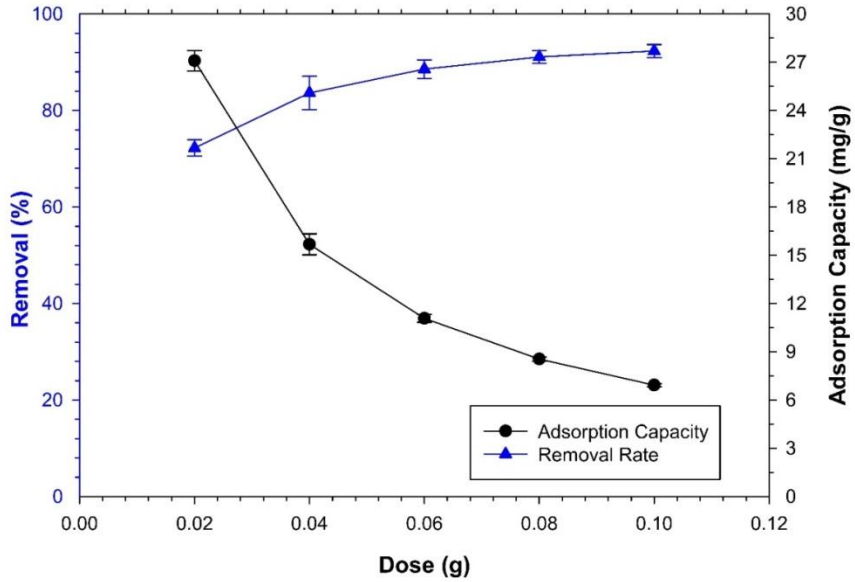

Figure 7: Impact of the GS's dose on the removal rate and adsorption capacity.

This numerical enhancement can be attributed to an augmented presence of vacant sites with uniform density, facilitating enhanced accessibility and greater exposed surface area [32]. On the other hand, a reduction in the adsorption capacity was simultaneously noticed as the removal rate increased, where the highest adsorption capacity reached 27.1 mg/g at 0.02 g and the lowest was obtained to be 6.92 mg/g at 0.1 g. Notably, when adsorbents are utilized in substantial quantities, interactions between them may occur, leading to reduced capacity due to clumping and clustering, resulting in a diminished overall surface area and a reduction in the adsorbance [33].

3.2.4. Effect of dye's initial concentration

The adsorption mechanism is notably impacted by the initial dye concentration, as the sorbent material's capacity is constant. In other words, the adsorption process is contingent on the dye concentration. In this study, a dye solution range of concentration from 10 to 50 mg/L was investigated while other operation parameters were fixed. The fixed parameters were: 0.06 g GS, 25 mL dye-solution, 30 min contact time, 350 rpm mixing speed, RT, and neutral pH. Figure 8 illustrates that as the dye concentration increases, the removal rate shows a modest decrease while almost a linear enhancement in the adsorption capacity takes place. In terms of numerical values, when a 10 ppm aqueous solution was utilized, the removal rate was 94.92 % and the adsorption capacity was 3.95 mg/g. However, these values were 78.84 % and 16.43 mg/g, respectively, when a 50 ppm dye-aqueous solution was studied. Previous research indicates that lower initial dye concentrations yield higher removal rate results due to an abundance of unoccupied binding sites, facilitating efficient and swift adsorption [34]. Conversely, elevated dye quantities may lead to competition among molecules for available sites, causing saturation and diminished removal efficiency [35]. The reverse scenario is observed when we talk about the adsorption capacity but for the same reasonable cause. The removal rate results appear to reach near equilibrium at 40 ppm with almost no change with 50 ppm, while the adsorption capacity showed a continuous rise. In normal situations, the capacity also reaches its maximum as initially empty binding sites on the particles are available for dye absorption, but over time, the adsorption rate slows as these sites become increasingly occupied. In our case, the adsorption capacity still increasing, which suggests the abundancy of adsorption sites and its reliability for the process [36].

3.2.5. Effect of temperature

The investigation into the impact of solution temperature on the elimination rate involved testing four distinct temperatures: 25, 35, 45, and 55 °C, while other parameters are fixed. These parameters include a dye concentration of 30 ppm, solution volume of 25 mL, mixing speed of 350 rpm, natural pH, contact

time of 30 min, and adsorbent dose of 0.06 g. Figure 9 illustrates the influence of these temperatures on the removal rate and adsorption capacity. The graphical representation indicates a marginal decrease in the examined parameters as the temperature rises. These findings suggest that the process is neither endothermic nor exothermic, where an identical behavior for the removal rate and adsorption capacity. Commonly, higher temperatures enhance the bonding forces between the adsorbed substance and the adsorbent material [37]. Yet, the bonding in our research showed an independent function on temperature.

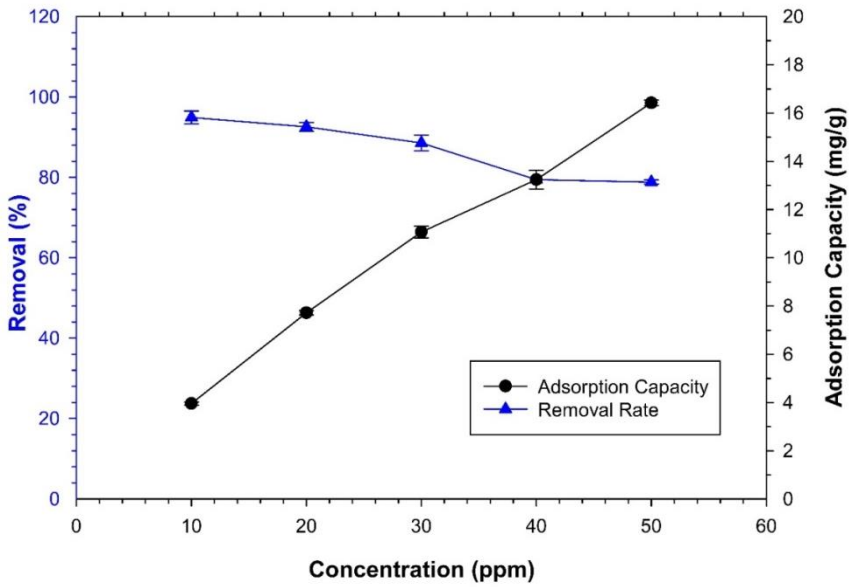

Figure 8: The effect of dye's initial concentration on the removal rate and adsorption capacity.

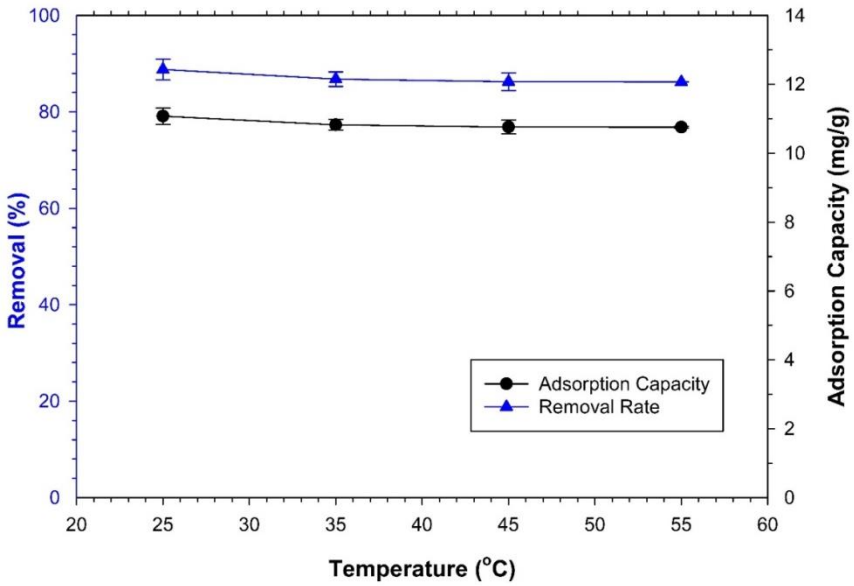

Figure 9: Effect of Temperature on the removal rate and adsorption capacity.

3.3. Theoretical analysis

3.3.1. Isotherm study

Understanding the interaction between the adsorbent and adsorbate during the adsorption process is crucial, and a key aspect of this comprehension involves the analysis of isotherms. Various types of adsorption isotherms aid in identifying the phenomena and providing an explanation for its considerations. Nevertheless, specific models are commonly employed due to their compatibility with the data. In our study,

we opted for the most widely recognized isotherms, namely Langmuir, Freundlich, and Temkin. Practical measurements were compared with the expected model results to determine the most suitable model. The model exhibiting the highest coefficient of determination (R^2) effectively elucidated the adsorption mechanism [24].

The Langmuir isotherm presents the maximum adsorption capacity achievable by a monolayer of adsorbent. It suggests the creation of a uniform monolayer with a finite adsorption capacity. Once the adsorption sites are occupied by adsorbate molecules, any additional uptake of molecules on these sites is hindered. The following equation mathematically represents the Langmuir model (Eq. 3):

$$q = \frac{q_{max} \times K_L \times C_e}{1 + K_L \times C_e} \quad (3)$$

In the provided context, q signifies the adsorption capacity, q_{max} denotes the highest dye adsorbed on GS's surface (measured in milligrams per gram), K_L is a constant associated with adsorption-free energy (in liters per milligram), and Ce represents the equilibrium concentration of the dye (in milligrams per liter). K_L's value is inversely proportional to adsorption free energy, indicating that a decrease in K_L corresponds to an increased tendency of the adsorbate to bind to the adsorbent. The Langmuir model can be linearly expressed through equation 4, and by plotting C_e/q against C_e, the slope and intercept of the graph can be used to estimate q_{max} and K_L, respectively [38].

$$\frac{C_e}{q} = \frac{1}{q_{max} \times K_L} + \frac{C_e}{q_{max}} \quad (4)$$

The Freundlich model is effective in explaining heterogeneous adsorption processes involving multiple layers. With an enhancement in the concentration of the MB, there is a concurrent increase in the amount of adsorption. Equation 5 represents the mathematical expression for the isotherms.

$$q = K_f \times C_e^{(\frac{1}{n})} \quad (5)$$

K_f and n are constants linked to the adsorbate and adsorbent at a particular temperature.

Determination of these constants involves plotting the natural logarithms of q and C_e, resulting in a linear relationship described by equation 5. In this equation, the slope represents the value of K_f, while the intercept corresponds to 1/n. As per the equation, an increase in the values of these constants implies an enhancement in adsorption capacity [39].

The Temkin isotherm, the final model discussed, relies on the analysis of adsorption heat and is sensitive to the extent of adsorbate molecule coverage. As the amount of adsorbate molecules in the adsorption layer increases, the adsorption heat decreases linearly. Additionally, it is assumed that the adsorption binding energy remains constant across the adsorbent surfaces, enabling the achievement of maximum uptake energy. Equation 6 offers an estimation of the adsorption capacity.

$$q_e = \frac{RT}{b_T} \, lnK_T C_e \quad (6)$$

The equation signifies the connection between the mass of adsorbate and adsorbent, denoted as q_e (mg/g). K_T is the equilibrium binding constant associated with the maximum uptake (L/g). C_e represents the MB's concentration at equilibrium (mg/L), and b_T is the constant in the Temkin model related to adsorption heat (kJ/mol). To facilitate estimations, the above equation can be linearly expressed, as demonstrated in equation 7 [40].

$$q_e = BlnK_T + BlnC_e \quad (7)$$

Where $B = \frac{RT}{b_T}$

In Figures 10a, b, and c, the adsorption data of MB dye on GS are presented based on the Langmuir, Freundlich, and Temkin isotherms, respectively. Notably, the Langmuir model exhibits the highest R^2 in the figure, assuming that the adsorption process is dominated by a single layer and physical bonding. All statistical information was illustrated in Table S1.

Table 1: The isotherm models parameters' values.

Langmuir			Freundlich			Temkin			
q_{max} mg/g	K_L (L/mg)	R^2	K_f	n	R^2	K_t L/g	q_T mg/g (RT/b_T)	b_T KJ/mol, RT/q_T	R^2
16.8067	0.601	0.996	5.8487	2.2815	0.9674	5.2948	3.8119	0.6499	0.9731

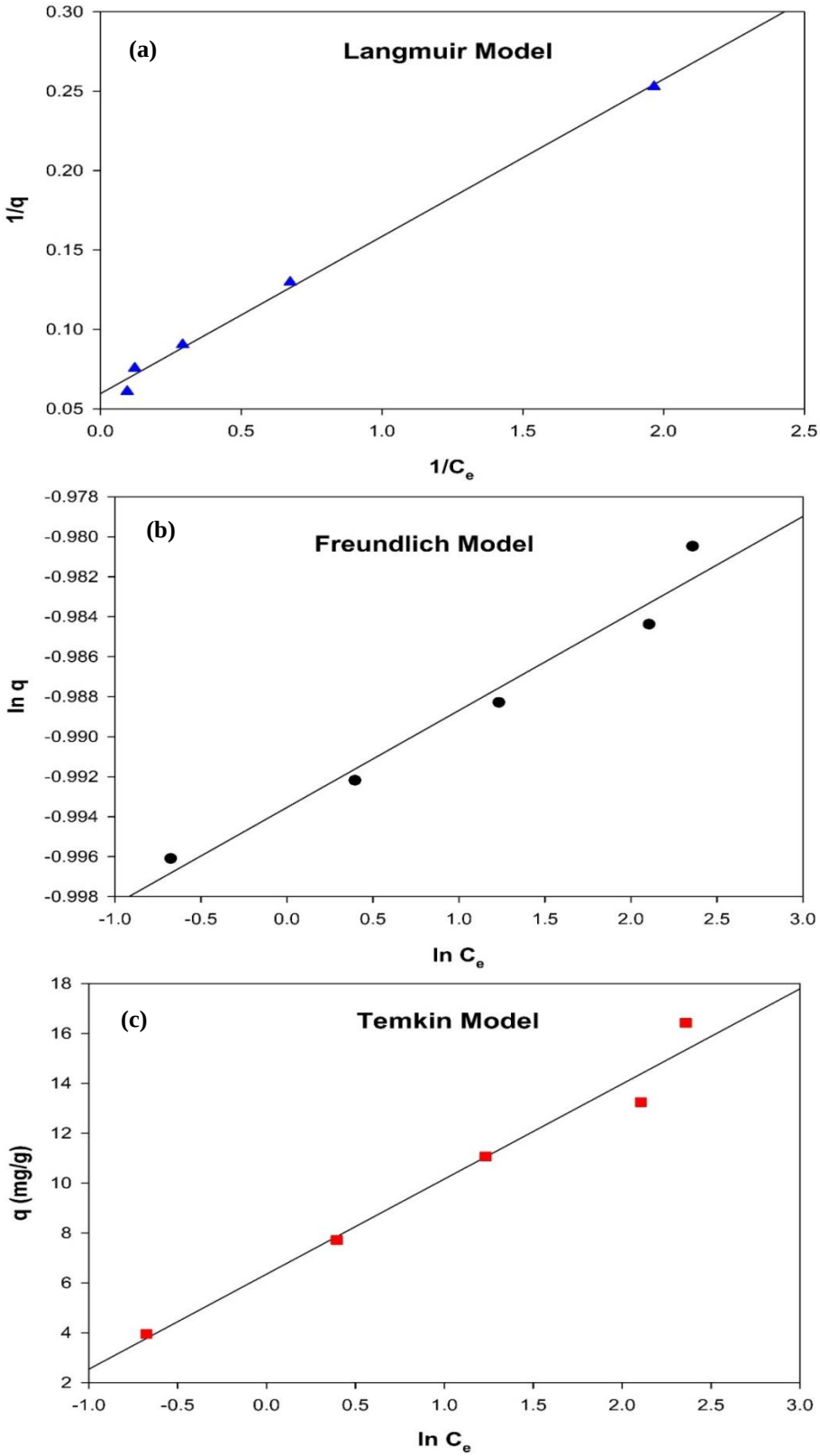

Figure 10: The isotherm models of adsorption, (a) Langmuir, (b) Freundlich, and (c) Temkin.

However, the other two models, Freundlich and Temkin, showed also relatively high R^2 values of 0.9674 and 0.9731, respectively, which make them unignorable. Thereby, more than one scenario could be applicable. In the Freundlich model, the binding is chemical and the adsorption is in the multilayer form. Moreover, the value of n is 2.2815, signifying a substantial level of adsorption on GS surfaces. Put differently, effective adsorption is observed when the value of 1/n falls within the range of 0.1 to 1. In our study, the calculated 1/n value is 0.438, indicating that 44 % of the active adsorption sites possess identical energy levels [41]. The observed adsorption is attributed to the robust electrostatic charge of GSs and their distinctive structure [42].

The Temkin model posits that adsorption is a multi-layer process, disregarding significantly elevated or diminished amounts of the adsorbate in the liquid phase. It was confirmed that the differential heat of adsorption decreases linearly as the coverage increases and the interaction of the adsorbent-adsorbate is weak [43]. Table 1 shows a summary of the model's parameter values, while Table S1 shows a statistical analysis of the three models.

3.3.2. Kinetics study

Understanding adsorption kinetics is essential for comprehending both the mechanism and rate of the adsorption process. Various models, each based on different assumptions, aim to elucidate the mechanism of adsorption. For this specific purpose, we have selected five commonly used models: the pseudo-zero-order, pseudo-first-order, pseudo-second-order, Elovich, and intraparticle diffusion models. To determine the most appropriate model, we computed the R^2 for each model to assess its alignment with the practical data. The R^2 values for the pseudo-zero-order, pseudo-first-order, pseudo-second-order, Elovich, and intraparticle diffusion models were found to be 0.9703, 0.6283, 0.9998, 0.8883, and 0.9372, respectively. Based on the analysis, it can be inferred that the models performed optimally in the following order: pseudo-second-order, pseudo-zero-order, intraparticle diffusion, Elovich, and pseudo-first-order. The statistical analysis of the five models was illustrated in Table S2, where the adjusted R^2 values followed the same order of R^2. Consequently, we will focus our examination on the model with the highest R^2 value, namely the pseudo-second-order.

Our results perfectly align with the pseudo-second-order model, assuming that the adsorption rate is not influenced by concentration but is determined by adsorption capacity. This model considers the potential limitation of chemisorption rate on adsorption, possibly due to surface group quantity. In fact, the pseudo-second-order model accurately predicts the equilibrium adsorption capacity, as demonstrated by Sahoo and Prelot [44]. The relationships between the models' calculations are depicted in Figure 11.

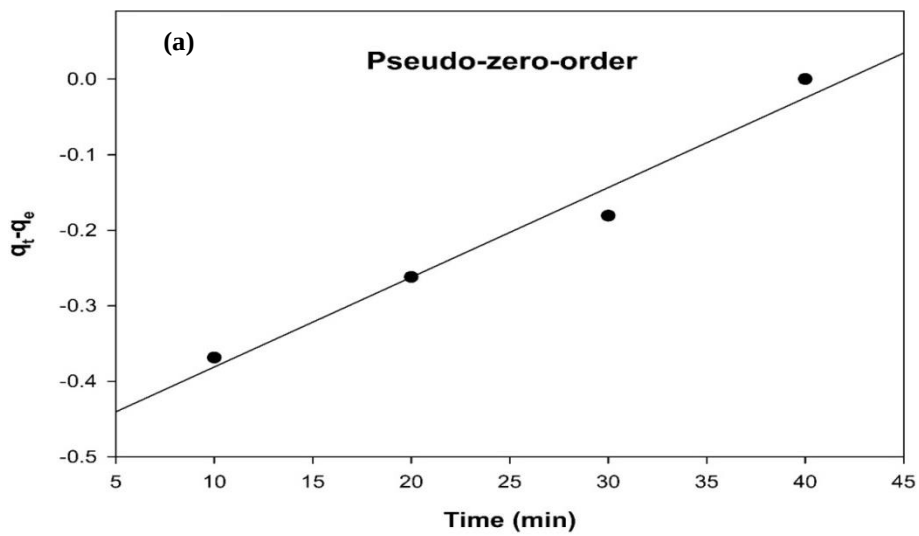

Figure 11: Kinetics models of the adsorption, (a) Pseudo zero order, (b) Pseudo first order, (c) Pseudo second order, (d) Elovich, and (e) Intraparticle diffusion model.

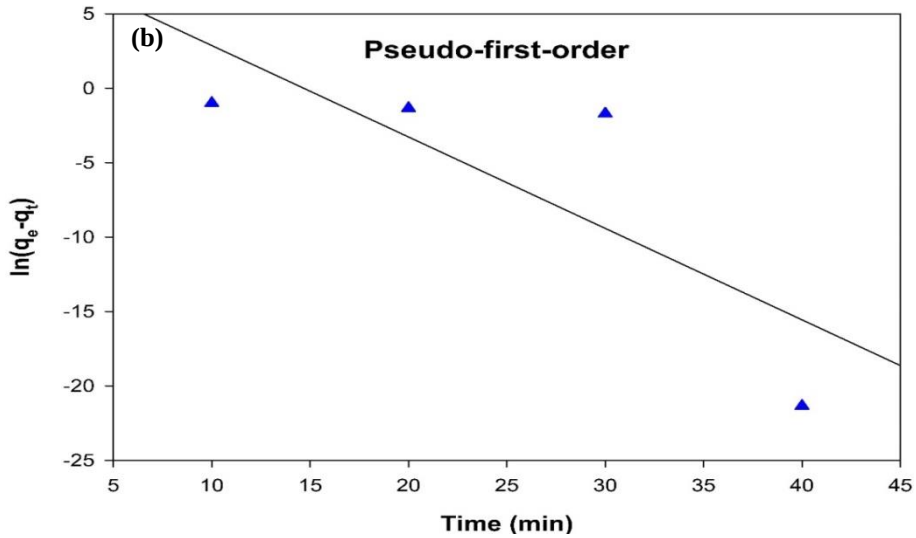

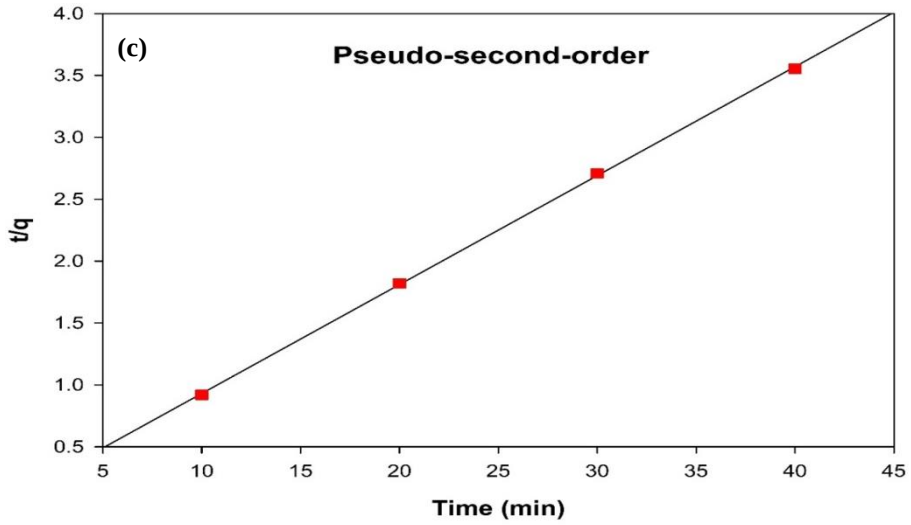

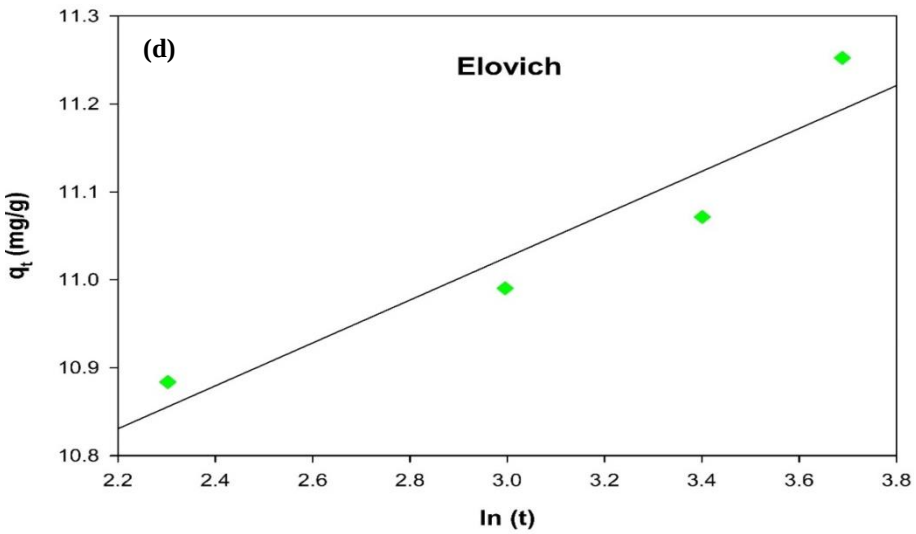

Figure 11: Continue.

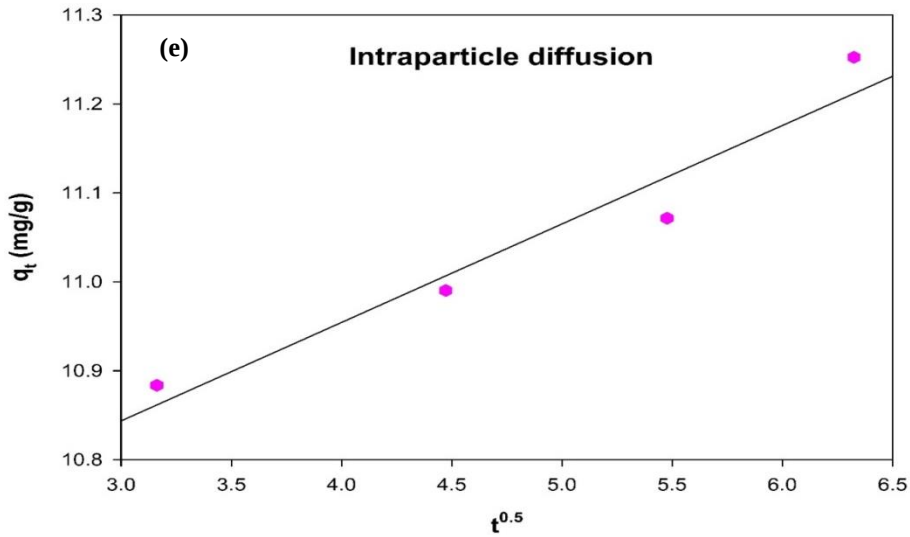

Figure 11: Continue.

The adsorption mechanism of the GS employed for methylene blue removal entails the movement of methylene blue molecules from the aqueous solution to the surface of the adsorbent. Subsequently, these molecules chemically bond with active sites on the adsorbent, resulting in the formation of a monolayer that adheres to the Langmuir isotherm. This phenomenon is defined by the presence of adsorption sites that have the same capacity and become fully occupied once equilibrium is reached. The pseudo second order kinetics model states that the rate-limiting step is the chemisorption process.

In the end, we suggested the comparison of our results with similar biowaste adsorbents, where the GS shows a remarkable adsorption capacity and is set as a powerful adsorbent as illustrated in Table 2. It is good to mention two points, first is some compared wastes might be advanced treated, while the GS was simply used. The second is the GS performance is even higher than some other biochar materials, but we didn't include them to keep the constancy. Here, it can be stated that plain GS shows a very high performance, in addition to being simple, sustainable, abundant, and cheap.

Table 2: A comparison of adsorption capacities of different adsorbents for MB dye.

Adsorbent	Adsorption Capacity (mg/g)	Reference
Gundelia seeds waste	30.57	This work
Wheat shells	4.23	[45]
Orange peels	18.6	[46]
Catton waste	24.0	[47]
Jute processing waste	22.47	[48]
Banana peel	20.8	[46]
Cereal chaff	20.3	[49]
Wheat shells	16.56	[50]
Raw beech sawdust	9.78	[51]
Spent coffee grounds	18.7	[52]
Neem saw dust	3.62	[53]
Beer brewery waste	4.92	[54]

4. Conclusion

In conclusion, this study highlights the promising potential of GS waste as an environmentally friendly and effective adsorbent for the removal of MB dye from contaminated water. Through meticulous experimentation and analysis, we have elucidated various factors influencing the adsorption process, including pH, dose, initial dye concentration, and temperature. Our investigation into the effect of pH revealed that near-neutral conditions (pH=7) yield optimal removal rates and adsorption capacities. The point of zero charge (PZC) of GS was determined to be at pH=8, providing valuable insight into its surface charge characteristics. Moreover, the dose of GS significantly influenced both the removal rate and adsorption capacity, with higher doses yielding increased removal rates but reduced adsorption capacities due to clustering effects. Furthermore, we observed that the initial dye concentration has a notable impact on the adsorption process; lower concentrations resulted in higher removal rates, while higher concentrations led to increased adsorption capacities. The effect of temperature on the adsorption process was found to be marginal, indicating that the process is neither endothermic nor exothermic. Theoretical analyses using Langmuir, Freundlich, and Temkin isotherm models provided valuable insights into the adsorption mechanism. The Langmuir model exhibited the best fit to the experimental data, suggesting monolayer adsorption with physical bonding. However, the Freundlich and Temkin models also displayed high R^2 values, indicating potential multilayer adsorption with chemical bonding. Additionally, kinetics studies revealed that the pseudo-second-order model best describes the adsorption process, indicating that adsorption capacity rather than concentration primarily governs the rate of adsorption. This finding underscores the importance of considering chemisorption mechanisms in understanding the adsorption kinetics. Ultimately, this study shows that GS waste may be used as a sustainable and effective dye adsorbent in wastewater treatment applications, supporting environmental rehabilitation and waste valorization. To prove GS-based adsorption techniques' practicality and scalability, optimization and practical uses might be studied.

Acknowledgment

The authors like to thank the Department of Chemical Engineering at the University of Baghdad for partially supporting this work.

5. References

1. Ahmed AU, Ibraheem H, Kadhom M, Rashad AA, Al-Dahhan WH, Bufaroosha M, et al. Modified PVC as adsorbent for methyl orange dye removable, 2022, p. 020006. https://doi.org/10.1063/5.0093582.
2. Ismail Z, Go YI. Fog-to-Water for Water Scarcity in Climate-Change Hazards Hotspots: Pilot Study in Southeast Asia. Global Challenges 2021; 5. https://doi.org/10.1002/gch2.202000036.
3. Droogers P, Immerzeel WW, Terink W, Hoogeveen J, Bierkens MFP, van Beek LPH, et al. Water resources trends in Middle East and North Africa towards 2050. Hydrol Earth Syst Sci. 2012; 16:3101-14. https://doi.org/10.5194/hess-16-3101-2012.
4. Karadag D, Akgul E, Tok S, Erturk F, Kaya MA, Turan M. Basic and reactive dye removal using natural and modified zeolites. J Chem Eng Data. 2007; 52:2436-41. https://doi.org/10.1021/je7003726.
5. Silva F, Nascimento L, Brito M, da Silva K, Paschoal W, Fujiyama R. Biosorption of Methylene Blue Dye Using Natural Biosorbents Made from Weeds. Materials. 2019; 12:2486. https://doi.org/ 10.3390/ ma12152486.
6. Küçükosmanoğlu M, Gezici O, Ayar A. The adsorption behaviors of Methylene Blue and Methyl Orange in a diaminoethane sporopollenin-mediated column system. Sep Purif Technol. 2006; 52:280-7. https://doi.org/10.1016/j.seppur.2006.05.005.
7. Oladoye PO, Kadhom M, Khan I, Hama Aziz KH, Alli YA. Advancements in adsorption and photodegradation technologies for rhodamine B dye wastewater treatment: Fundamentals, applications, and future directions. Green Chem Eng. 2023; https://doi.org/10.1016/j.gce.2023.12.004.
8. Salih SS, Mohammed HN, Abdullah GH, Kadhom M, Ghosh TK. Simultaneous removal of Cu(II), Cd(II), and industrial dye onto a composite chitosan biosorbent. J Polym Environ. 2020; 28:354-65. https://doi.org/10.1007/ s10924-019-01612-x.
9. Salih SS, Mahdi A, Kadhom M, Ghosh TK. Competitive adsorption of As(III) and As(V) onto chitosan/diatomaceous earth adsorbent. J Environ Chem Eng. 2019; 7:103407. https://doi.org/10.1016/j.jece.2019.103407.
10. Jawad AH, Kadhum AM, Ngoh YS. Applicability of dragon fruit (Hylocereus polyrhizus) peels as low-cost biosorbent for adsorption of methylene blue from aqueous solution: kinetics, equilibrium and

thermodynamics studies. Desalination water treat 2018; 109:231-40. https://doi.org/10.5004/dwt.2018.21976.
11. Adil H, Hussain Z, Kadhom M, Yousif E. Adsorptive removal of safranin-O dye from aqueous solutions using carrot seed, 2022, p. 040011. https://doi.org/10.1063/5.0121105.
12. Salih SS, Kadhom M, Shihab MA, Ghosh TK. Competitive adsorption of Pb(II) and phenol onto modified chitosan/vermiculite adsorbents. J Polym Environ. 2022; 30:4238-51. https://doi.org/10.1007/s10924-022-02515-0.
13. Boakye P, Ohemeng-Boahen G, Darkwah L, Sokama-Neuyam YA, Appiah-Effah E, Oduro-Kwarteng S, et al. Waste biomass and biomaterials adsorbents for wastewater treatment. Green Energy Enviro Technol. 2022; 2022:1–25. https://doi.org/10.5772/geet.05.
14. Moussavi G, Mahmoudi M. Removal of azo and anthraquinone reactive dyes from industrial wastewaters using MgO nanoparticles. J Hazard Mater. 2009;168:806-12. https://doi.org/10.1016/j.jhazmat. 2009. 02.097.
15. Alalwan HA, Kadhom MA, Alminshid AH. Removal of heavy metals from wastewater using agricultural byproducts. J Water Supply: Res Technol-AQUA. 2020; 69:99-112. https://doi.org/10.2166/aqua. 2020. 133.
16. Kadhom M, Albayati N, Alalwan H, Al-Furaiji M. Removal of dyes by agricultural waste. Sustain Chem Pharm. 2020; 16. https://doi.org/10.1016/j.scp. 2020. 100259.
17. Dalar A, Zengin G, Mukemre M, Bengu AS, İşler S. Gundelia rosea seed: Evaluation of biopharmaceutical potential and bioactive composition. South African J Botany. 2019; 125:505-10. https://doi.org/10.1016/j.sajb.2019.08.024.
18. Hind N. 763. GUNDELIA TOURNEFORTII. Curtis's Botanical Magazine 2013;30:114-38. https://doi.org/10.1111/curt.12027.
19. Golshan Shandi S, Doulati Ardejani F, Sharifi F. Assessment of Cu (II) removal from an aqueous solution by raw Gundelia tournefortii as a new low-cost biosorbent: Experiments and modelling. Chin J Chem Eng. 2019; 27:1945-55. https://doi.org/10.1016/j.cjche. 2018.12.027.
20. Rahimpour F, Shojaeimehr T, Sadeghi M. Biosorption of Pb(II) using *Gundelia tournefortii*: Kinetics, equilibrium, and thermodynamics. Sep Sci Technol. 2017; 52:596-607. https://doi.org/10.1080/01496395. 2016.1260140.
21. Mokhtaryan S, Khodabakhshi A, Sadeghi R, Nourmoradi H, Shakeri K, Hemati S, et al. New activated carbon derived from Gundelia tournefortii seeds for effective removal of acetaminophen from aqueous solutions: Adsorption performance. Arabian J Chem. 2023; 16:105253. https://doi.org/10.1016/j.arabjc. 2023. 105253.
22. Pezeshkvar T, Norouzi B, Moradian M, Mirabi A. Fabrication of new nanocomposites based on NiO-MWCNT-sodium dodecyl sulfate in the presence of Gundelia tournefortii extract: application for methanol electrooxidation in alkaline solution. J Solid State Electrochem. 2022; 26:1479-92. https://doi.org/10.1007/s10008-022-05182-2.
23. Cwalinski T, Polom W, Marano L, Roviello G, D'Angelo A, Cwalina N, et al. Methylene Blue—Current Knowledge, Fluorescent Properties, and Its Future Use. J Clin Med. 2020; 9:3538. https://doi.org/10.3390/jcm9113538.
24. Kadhom M, Kalash K, Al-Furaiji M. Performance of 2D MXene as an adsorbent for malachite green removal. Chemosphere. 2022; 290:133256. https://doi.org/10.1016/j.chemosphere.2021.133256.
25. Ovchinnikov O V., Evtukhova A V., Kondratenko TS, Smirnov MS, Khokhlov VYu, Erina O V. Manifestation of intermolecular interactions in FTIR spectra of methylene blue molecules. Vib Spectrosc. 2016; 86:181-9. https://doi.org/10.1016/j.vibspec. 2016. 06.016.
26. Sartape AS, Mandhare AM, Jadhav VV., Raut PD, Anuse MA, Kolekar SS. Removal of malachite green dye from aqueous solution with adsorption technique using Limonia acidissima (wood apple) shell as low cost adsorbent. Arabian J Chem. 2017; 10:S3229-38. https://doi.org/10.1016/j.arabjc.2013.12.019.
27. Kumar R, Ahmad R. Biosorption of hazardous crystal violet dye from aqueous solution onto treated ginger waste (TGW). Desalination. 2011; 265:112-8. https://doi.org/10.1016/j.desal.2010.07.040.
28. [28]Shamsipur M, Barati A, Nematifar Z. Fluorescent pH nanosensors: Design strategies and applications. J Photochem Photobiol C: Photochem Rev. 2019; 39:76-141. https://doi.org/10.1016/j.jphotochemrev.2019. 03. 001.
29. Bella F, Gerbaldi C, Barolo C, Grätzel M. Aqueous dye-sensitized solar cells. Chem Soc Rev. 2015; 44:3431-73. https://doi.org/10.1039/C4CS00456F.
30. [30]Alvarez-Silva M, Uribe-Salas A, Mirnezami M, Finch JA. The point of zero charge of phyllosilicate minerals using the Mular–Roberts titration technique. Miner Eng. 2010; 23:383-9. https://doi.org/10.1016/j.mineng.2009.11.013.
31. Luo H, Liu Y, Lu H, Fang Q, Rong H. Efficient adsorption of tetracycline from aqueous solutions by modified alginate beads after the removal of Cu(II) Ions. ACS Omega. 2021; 6:6240-51. https://doi.org/10.1021/acsomega.0c05807.
32. Silva F, Nascimento L, Brito M, da Silva K, Paschoal W, Fujiyama R. Biosorption of methylene blue dye using natural biosorbents made from weeds. Materials. 2019; 12:2486. https://doi.org/10.3390/ma12152486.
33. Singh P, Sarswat A, Pittman CU, Mlsna T, Mohan D. Sustainable low-concentration arsenite [As(III)] removal in single and multicomponent systems using hybrid iron oxide–biochar nanocomposite adsorbents-a mechanistic study. ACS Omega. 2020; 5:2575-93. https://doi.org/10.1021/acsomega.9b02842.
34. Muthukumaran C, Sivakumar VM, Thirumarimurugan M. Adsorption isotherms and kinetic studies of crystal

violet dye removal from aqueous solution using surfactant modified magnetic nanoadsorbent. J Taiwan Inst Chem Eng. 2016; 63:354-62. https://doi.org/10. 1016/ j.jtice.2016.03.034.
35. S R, Lata S, P B. Biosorption characteristics of methylene blue and malachite green from simulated wastewater onto Carica papaya wood biosorbent. Surfaces Interfaces. 2018; 10:197-215. https://doi.org/ 10. 1016/j.surfin.2017.09.011.
36. Zhou G, Wang KP, Liu HW, Wang L, Xiao XF, Dou DD, et al. Three-dimensional polylactic acid@ graphene oxide/chitosan sponge bionic filter: Highly efficient adsorption of crystal violet dye. Int J Biol Macromol. 2018; 113:792-803. https://doi.org/10. 1016/ j.ijbiomac.2018.02.017.
37. Boudrahem F, Aissani-Benissad F, Soualah A. Removal of basic yellow dye from aqueous solutions by sorption onto reed as an adsorbent. Desalination Water Treat. 2014:1-8. https://doi.org/10.1080/ 19443994. 2014.888686.
38. Jiang N, Shang R, Heijman SGJ, Rietveld LC. Adsorption of triclosan, trichlorophenol and phenol by high-silica zeolites: Adsorption efficiencies and mechanisms. Sep Purif Technol. 2020; 235:116152. https://doi.org/10.1016/j.seppur.2019.116152.
39. Li L, Wang X, Zhang D, Guo R, Du X. Excellent adsorption of ultraviolet filters using silylated MCM-41 mesoporous materials as adsorbent. Appl Surf Sci. 2015; 328:26-33. https://doi.org/10.1016/j.apsusc. 2014. 11.116.
40. Foo KY, Hameed BH. Insights into the modeling of adsorption isotherm systems. Chem Eng J. 2010; 156:2-10. https://doi.org/10.1016/j.cej.2009.09.013.
41. Vidal CB, Barros AL, Moura CP, de Lima ACA, Dias FS, Vasconcellos LuizCG, et al. Adsorption of polycyclic aromatic hydrocarbons from aqueous solutions by modified periodic mesoporous organosilica. J Colloid Interface Sci. 2011; 357:466-73. https://doi.org/10.1016/j.jcis.2011.02.013.
42. Kalash KR, Al-Furaiji MH, Waisi BI, Ali RA. Evaluation of adsorption performance of phenol using non-calcined Mobil composition of matter No. 41 particles. Desalination Water Treat. 2020; 198:232-40. https://doi.org/10.5004/dwt.2020.26018.
43. Yang C. Statistical mechanical aspects of adsorption systems obeying the Temkin isotherm. J Phys Chem. 1993; 97:7097-101. https://doi.org/10.1021/j100129a 029.
44. Sahoo TR, Prelot B. Adsorption processes for the removal of contaminants from wastewater. Nanomaterials for the detection and removal of wastewater pollutants. Elsevier; 2020, p. 161-222. https://doi.org/10.1016/B978-0-12-818489-9.00007-4.
45. Banerjee S, Chattopadhyaya MC, Uma, Sharma YC. Adsorption Characteristics of Modified Wheat Husk for the Removal of a Toxic Dye, Methylene Blue, from Aqueous Solutions. J Hazard Toxic Radioact Waste. 2014; 18:56-63. https://doi.org/10.1061/ (ASCE) HZ. 2153-5515.0000191.
46. ANNADURAI G, JUANG R, LEE D. Use of cellulose-based wastes for adsorption of dyes from aqueous solutions. J Hazard Mater. 2002; 92:263-74. https://doi.org/10.1016/S0304-3894(02)00017-1.
47. Yavuz E, Bayramoğlu G, Arica MY, Senkal BF. Preparation of poly (acrylic acid) containing core-shell type resin for removal of basic dyes. J Chem Technol Biotechnol. 2011; 86:699-705. https://doi.org/10. 1002/jctb.2571.
48. Banerjee S, Dastidar MG. Use of jute processing wastes for treatment of wastewater contaminated with dye and other organics. Bioresour Technol. 2005; 96:1919-28. https://doi.org/10.1016/j.biortech.2005. 01. 039.
49. Han R, Wang Y, Han P, Shi J, Yang J, Lu Y. Removal of methylene blue from aqueous solution by chaff in batch mode. J Hazard Mater. 2006; 137:550-7. https://doi.org/10.1016/j.jhazmat.2006.02.029.
50. Bulut Y, Aydın H. A kinetics and thermodynamics study of methylene blue adsorption on wheat shells. Desalination. 2006; 194:259-67. https://doi.org/10. 1016/j.desal.2005.10.032.
51. BATZIAS F, SIDIRAS D. Dye adsorption by calcium chloride treated beech sawdust in batch and fixed-bed systems. J Hazard Mater. 2004; 114:167-74. https://doi.org/10.1016/j.jhazmat.2004.08.014.
52. Franca AS, Oliveira LS, Ferreira ME. Kinetics and equilibrium studies of methylene blue adsorption by spent coffee grounds. Desalination. 2009; 249:267-72. https://doi.org/10.1016/j.desal.2008.11.017.
53. Khattri SD, Singh MK. Colour removal from synthetic dye waste water using a bioadsorbent. Water Air Soil Pollut. 2000; 120:283-94. https://doi.org/10. 1023/ A:1005207803041.
54. Tsai WT, Hsu H-C, Su TY, Lin KY, Lin CM. Removal of basic dye (methylene blue) from wastewaters utilizing beer brewery waste. J Hazard Mater. 2008; 154:73-8. https://doi.org/10.1016/j.jhazmat. 2007. 09.107.

How to cite this article:
Albayati N, Mohammed M, Ahmed H, Kadhom M.The Potential of Gundelia Seeds Waste as an Emerging Sustainable Adsorbent for Methylene Blue-Polluted Water Treatment. Prog Color Colorants Coat. 2025;18(1):53-71. https://doi.org/ 10.30509/pccc.2024.167290.1285.